

## CHAPTER 3

# FLOW PATTERNS AND WALL SHEAR STRESS IN ARTERIES

### 1 STRAIGHT TUBES

The next three chapters, which form the core of this monograph, have two main purposes. One is to give a theoretical explanation for some of the arterial velocity profiles described in § 1.2.4. The other, of greater potential importance in the analysis of arterial disease, is to make predictions of the detailed distribution of wall shear stress in arteries, which is related to the rate of mass transport across artery walls and hence (presumably) to atherogenesis (§ 1.2.6). The second purpose is particularly important because no method has yet been devised to measure wall shear stress accurately as a function of time *in vivo*. This is rather surprising, considering the probable importance of wall shear, and the first section of this chapter is devoted to an explanation of why it is so difficult to measure. The second section begins the analysis of viscous flow in arteries with a discussion of unsteady entry flow (with flow reversal) in a straight tube. In chapters 4 and 5 respectively, curved and branched tubes are considered, and chapter 5 concludes with a discussion of flow instability in arteries.

### 3.1 The difficulty of measuring wall shear stress

#### 3.1.1 *The need for a good frequency response*

Since the mechanism by which the wall shear stress influences mass transport across the artery wall is unknown, with the consequence that the relevant features of the wall shear distribution cannot be identified, it is important to understand as many features as possible. In particular, the time-dependence of the wall shear at various sites on the artery wall should be accurately recorded, because, as will be argued in § 3.2.3, the unsteady components are likely to be at least as important as the mean shear. We have seen in § 1.2.3 that there are devices that can measure the flow-rate through an artery,

and the local blood velocity at points within it, with adequate accuracy. That is, the time variation of these velocities can be faithfully recorded, except at times close to those at which the flow reverses its direction (see appendix). However, the requirements of a device to measure wall shear are more stringent for two reasons. One is that the shear on a tube wall may reverse its direction when the average and centre-line velocities do not; furthermore, it always has a phase lead over those velocities (except when the Womersley parameter  $\alpha$  (see (2.35)) is so small that the flow is quasi-steady). This is because the slow-moving fluid near the wall responds more readily to variations in the driving pressure gradient than the faster-moving fluid in the core. Thus the problems associated with reversal are more pronounced in the case of wall shear measurement. The less obvious, but probably more significant, difficulty is that a wall shear probe must respond accurately to higher frequencies than a centre-line-velocity probe whereas, as we shall see, the probes hitherto designed are less well able to respond to high frequencies.

The need for a very good frequency response in wall shear measurement can be seen from Womersley's solution for oscillatory flow in a long, rigid, circular tube (§ 2.2). If the applied pressure gradient is

$$\frac{dp}{dx} = - \sum_{n=0}^{\infty} G_n e^{in\omega t}, \quad (3.1a)$$

then the average velocity is

$$\bar{u} = \frac{G_0 a^2}{8\mu} + \frac{a^2}{i\mu} \sum_{n=1}^{\infty} \frac{G_n}{\alpha_n^2} [1 - F(\alpha_n)] e^{in\omega t}, \quad (3.1b)$$

the centre-line velocity is

$$u(0) = \frac{G_0 a^2}{4\mu} + \frac{a^2}{i\mu} \sum_{n=1}^{\infty} \frac{G_n}{\alpha_n^2} \left[ 1 - \frac{1}{J_0(i^{3/2}\alpha_n)} \right] e^{in\omega t}, \quad (3.1c)$$

and the wall shear stress is

$$\tau = \frac{G_0 a}{2} + \frac{a}{2} \sum_{n=1}^{\infty} G_n F(\alpha_n) e^{in\omega t}, \quad (3.1d)$$

where  $\alpha_n^2 = n\omega a^2/\nu$  and  $F(\alpha)$  is given by (2.37). Now we saw in § 1.2 that up to 10 harmonics are required to reproduce accurately the average velocity waveform in the canine aorta; this neglects Fourier modes whose amplitudes are less than about  $5 \text{ cm s}^{-1}$ , 10% of the amplitude of the largest mode (Patel *et al.*, 1963*a*). Equations (3.1*b* and *c*) indicate that the same accuracy is required for centre-line velocity, and thus that a hot-film velocity probe for use in a dog has to have a good response to frequencies up to about 20 Hz. However, the terms in equation (3.1*d*) for  $\tau$  have (for large  $\alpha_n$ ) an amplitude equal to  $\alpha_n (\propto n^{1/2})$  times those in (3.1*b* and *c*). Thus (a)  $G_n$  must diminish faster than  $n^{-1/2}$  for this to be convergent, and assuming that this is satisfied (b) the sum must be taken to significantly higher values of  $n$  to achieve the same accuracy. The precise value of  $n$  required cannot be predicted without a knowledge of  $G_n$  for  $n > 10$ , but it can be seen clearly that a shear-stress probe must have a much better frequency response than one measuring centre-line velocity.

An example of what is required in practice can be derived by calculating the wall shear from a known velocity waveform, either measured or predicted. Fig. 3.1(*a*) shows the waveform of average velocity in the left anterior descending coronary artery of a horse, as calculated from the computer programme of Rumberger & Nerem (1977) (a similar measured waveform was shown in fig. 1.18). The heart-rate was taken to be 1 Hz. Fig. 3.1(*b*) indicates how many Fourier components are needed for an accurate representation of the root-mean-square (r.m.s.) velocity and the peak velocity; it can be seen that 8 harmonics (8 Hz) are adequate for the r.m.s. velocity, while 30 harmonics (30 Hz) are needed for the peak. Fig. 3.2(*a*) shows the corresponding waveform of wall shear-rate, calculated from (3.1*b* and *d*) using (a) over 100 and (b) 50 Fourier components; fig. 3.2(*b*) shows the peak and r.m.s. values of wall shear-rate as functions of the number of Fourier components used. From these we can see that even 50 components are not enough to represent the peak shear, although 20 are adequate for the r.m.s. Note that while the twentieth component corresponds to a frequency of 20 Hz in the horse, it corresponds to 40 Hz in the dog. The peak shear stress in this example is about  $9 \text{ N m}^{-2}$  and the r.m.s. is  $1.8 \text{ N m}^{-2}$ , compared with the mean value of about  $0.6 \text{ N m}^{-2}$ .

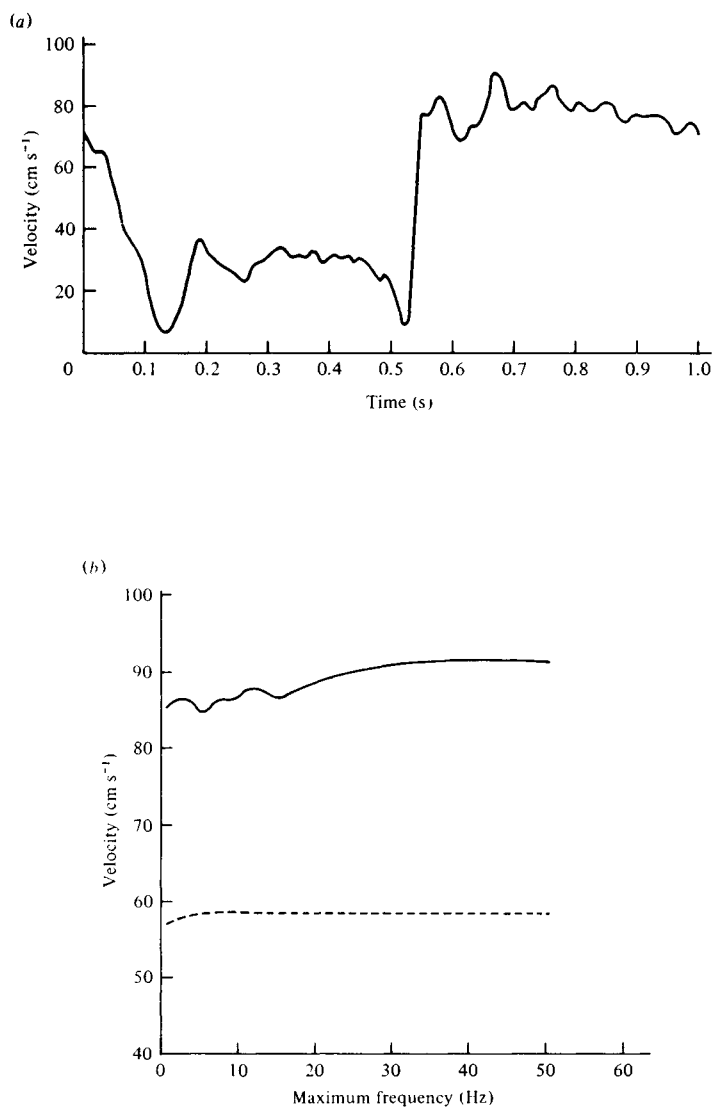


Fig. 3.1. (a) Calculated waveform of average velocity in the left anterior descending coronary artery of a horse.  $x = 25$  cm. (After Rumberger, 1976.) (b) Plots of peak (continuous curve) and r.m.s. (broken curve) velocities in a waveform reconstituted from a Fourier series of the waveform in (a), terminated after terms of a given frequency (abscissa).

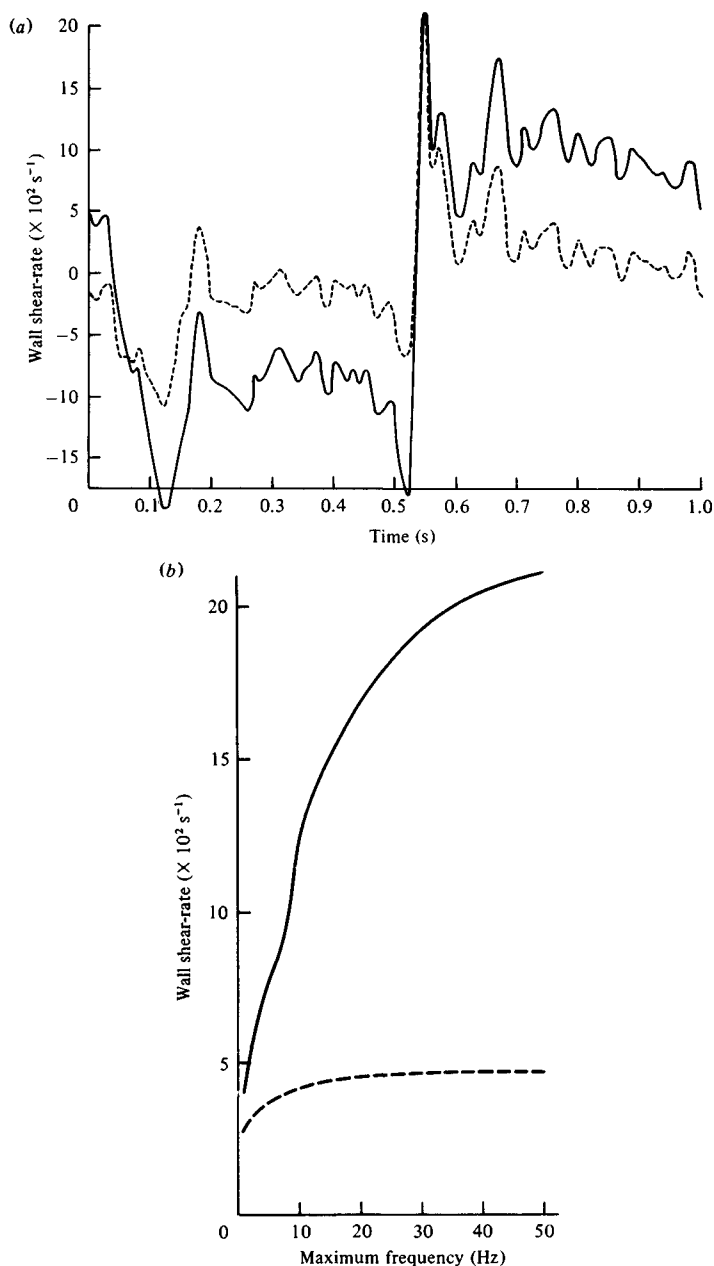


Fig. 3.2. (a) Calculated waveform of wall shear-rate in the left anterior descending coronary artery of a horse (continuous curve), together with the waveform reconstituted from the Fourier series, terminated at a frequency of 50 Hz (broken curve). (b) As for fig. 3.1(b), but for wall shear-rate not velocity. (I am most grateful to Mr T. Benson of the Ohio State University for performing the computations from which figs. 3.1 and 3.2 have been plotted.)

### 3.1.2 *The limitations of the hot-film anemometer*

One method of estimating wall shear in a tube is to measure the velocity profile at internal points and to extrapolate it to zero at the wall. However, this cannot be accurate unless there are several points within the inner part of the boundary layer on the wall, so that a smooth monotonic curve can be drawn through them. In arteries the unsteady boundary layers have thickness approximately equal to  $4(\nu/\omega)^{1/2}$ , where  $\omega$  is the angular frequency of the oscillations, and this takes a value of about 2.3 mm when the frequency is 2 Hz. The inner part of the boundary layer, in which the velocity profile is monotonic, is at most about 1 mm thick. Furthermore, both these numbers would be diminished for higher harmonics of the pulse. Now the hot-film anemometers used hitherto for velocity measurement are about 1 mm across, so it is difficult to make accurate measurements within the boundary layer. The only chance is to insert the probe in one wall of an artery and traverse the artery with the hot-film towards the far wall so that the film can enter the far boundary layer. Even so, accurate measurements cannot be made because of the radial excursion of the artery wall: the probe must remain far enough from the wall in systole not to be struck by it in diastole. Thus in the aortae of dogs (Seed & Wood, 1971; Clark & Schultz, 1973) measurements are not made in the boundary layer. The situation is somewhat better in horses, because of their lower heart-rate and, hence, thicker boundary layers, and Nerem *et al.* (1974a) have reported some measurements in the far boundary layer (without commenting on the problem of wall movement).

Other methods of measuring velocity profiles, e.g. with a catheter-tip electromagnetic flowmeter (Mills *et al.*, 1970), or by ultrasonic Doppler anemometry (Peronneau *et al.*, 1970), suffer from the same limitation of poor resolution, to within 1 mm. Similar limitations apply to flow in rigid transparent models, but in these the scale of the flow can be increased so that the probe width is a small fraction of the boundary layer thickness (also laser Doppler anemometry, which has somewhat finer resolution, is nowadays available). Even when the velocity profile is known quite accurately, extrapolation to estimate wall shear is notoriously inaccurate. Brech & Bellhouse (1973) reported a 50% discrepancy between such estimates and values measured directly by a hot-film probe

(but see below); Minton & Selvalingam (1970) have also shown a 25% discrepancy between this method and theoretical deduction for oscillatory flow in a long straight tube.

Thus one should attempt to measure wall shear stress another way. The only method at present available for use *in vivo* employs a constant-temperature hot-film embedded in the vessel wall, heat transfer from it being related to the local shear-rate. A variation of this method involving mass transfer from an electrode in a flowing electrolyte (the 'electrochemical technique') can also be used in model experiments (Reiss & Hanratty, 1962). Such probes have been used to measure the wall shear in steady flow in rigid models, ranging from two-dimensional branched channels (Smith, Colton & Freedman, 1974) to three-dimensional casts of the canine aorta (Lutz *et al.*, 1977), and yield satisfactory results. These authors also used their probes in sinusoidally oscillating flow, assuming that the quasi-steady calibration was applicable.

The behaviour of such shear probes is investigated theoretically in the appendix, on the assumption that two-dimensional boundary layer theory is applicable. This requires *both* that the Péclet number  $Pe = S_0 l^2 / \kappa$  is large (greater than about 400), where  $S_0$  is the mean wall shear-rate,  $l$  is the length of the hot film (or electrode) in the direction of motion and  $\kappa$  is the thermal (or concentration) diffusivity of the fluid ( $\kappa \approx 1.4 \times 10^{-7} \text{ m}^2 \text{ s}^{-1}$  for heat in blood), *and* that  $l$  is much less than the width of the film in the perpendicular direction. Neither condition is well satisfied in practice: for example, when  $S_0 = 320 \text{ s}^{-1}$  (as for a 0.5 cm artery with a mean velocity of  $20 \text{ cm s}^{-1}$  such as the horse coronary artery) and when  $l = 0.1 \text{ mm}$  (as for the smallest hot-films hitherto made), the Péclet number is only about 23; both larger and smaller values of  $S_0$  are encountered in arteries. Furthermore, hot-films are often made only 2.5 times as wide as they are long, so the three-dimensionality of the temperature field over the film may be important. Nevertheless, the conclusions of the theory are expected to give a qualitative indication of the frequency response of a hot-film shear probe.

Use of the probe requires that there is a unique relation between the rate of heat transfer from the film,  $Q$ , and the wall shear-rate,  $S$ . Steady boundary layer theory indicates that

$$Q = 0.81(\kappa^2 l^2 S)^{1/3} (T_1 - T_0) \rho c_p, \quad (3.2)$$

where  $T_1$  is the temperature of the film and  $T_0$ ,  $\rho$ ,  $c_p$  are the temperature, density and specific heat of the ambient fluid (L  v  que, 1928), although in any experiment the steady relation between  $Q$  and  $S$  would of course be measured directly. In order that the probe can be used in unsteady flow, therefore, its response must be known to be quasi-steady, i.e. (3.2) or its empirical equivalent must be known to be true at every instant. One of the main conclusions of the theory outlined in the appendix is that a hot-film shear probe will respond quasi-steadily to an unsteady shear  $S(t)$  as long as the quantity  $\lambda$  is small enough, where  $\lambda$  is defined by

$$\lambda = \left| \frac{3^{1/3} l^{2/3} dS/dt}{\kappa^{1/3} S^{5/3}(t)} \right|. \quad (3.3)$$

Numerical results suggest that 0.1 is the critical value above which  $\lambda$  should not rise. This makes it clear that as the shear approaches zero, prior to a flow reversal, the probe becomes completely inaccurate. Such inaccuracy is inevitable since the heat transfer from the film will be positive whatever the sign of the shear over it (and even in the complete absence of flow), so that it cannot fall to zero with the shear (see fig. A.10 in the appendix).

The requirement that  $\lambda < 0.1$  also demonstrates how the response will cease to be quasi-steady, in a flow of sufficiently large frequency and not too small amplitude, well before reversal of the shear, and even in the absence of shear reversal. Consider a sinusoidal shear variation,

$$S(t) = S_0(1 + \alpha_1 \cos \omega t), \quad (3.4)$$

for which

$$\lambda = \left| \frac{3^{1/3} l^{2/3} \omega \alpha_1 \sin \omega t}{\kappa^{1/3} S_0^{2/3} (1 + \alpha_1 \cos \omega t)^{5/3}} \right|. \quad (3.5)$$

The predicted heat transfer as a function of time is shown for various values of the amplitude parameter  $\alpha_1$  (both greater and less than 1) and the frequency parameter  $\omega_1 = \omega l^{2/3} / \kappa^{1/3} S_0^{2/3}$  in figs. A.11(a)–(c). The increasing departure from the quasi-steady response as  $\omega_1$  (and hence  $\lambda$  for given values of  $\alpha_1$  and  $\omega t$ ) increases is most marked. As a practical example, we once more take the horse coronary artery, with  $S = 320 \text{ s}^{-1}$  and  $\alpha_1 \approx 5$  (Nerem *et al.*,



1974a): the value of  $\alpha_1$  was estimated from the quoted values of the ratio of maximum to mean velocity and of the Womersley parameter, using equations (3.1);  $l$  will again be taken to be 0.1 mm. A reasonable criterion for the usefulness of the hot-film output is that it should be quasi-steady for at least a quarter of a cycle around the time of peak shear, i.e.  $-\frac{1}{4}\pi \leq \omega t \leq \frac{1}{4}\pi$ . Equation (3.5) shows that, when  $\omega t = \frac{1}{4}\pi$ ,  $\lambda \approx 0.0036\omega$ ; thus  $\lambda < 0.1$ , and the probe can be used, only as long as the frequency  $f (= \omega/2\pi)$  is below 4.5 Hz. We have seen that this is not good enough for accurate wall shear measurements in the coronary arteries, even discounting the greater inaccuracy at times closer to flow reversal. If we were to require comparable accuracy for reversed shear, at  $\omega t = \frac{3}{4}\pi$ , the critical frequency would be reduced to 2 Hz. If we took  $\alpha_1 = 0.5$ , the critical frequency for accuracy at  $\omega t = \frac{1}{4}\pi$  would be 6 Hz, although in that non-reversing case the maximum value of  $\lambda$  would be less than 0.5 only if  $f < 2.5$  Hz. For a different example we consider a sinusoidal oscillation typical of the aorta of a dog, at a distance of 5 cm from the entrance (as analysed in § 3.2 below). Here  $S_0$  is smaller ( $= 80 \text{ s}^{-1}$ ) but  $\alpha_1$  is greater ( $\approx 50$ ): in this case the critical frequency for accuracy at  $\omega t = \frac{1}{4}\pi$  is 5.6 Hz. Once more, this does not represent an adequate frequency response. The only way open to an experimentalist to improve the frequency response, i.e. to reduce  $\lambda$  for a given shear distribution at a given time, is to make  $l$  smaller. However, the value of 0.1 mm used here for  $l$  is the smallest length of hot-film employed to date; new methods of probe construction are therefore required. The claim by Ling *et al.* (1968) to have measured wall shear *in vivo*, in the aorta of a dog, and to be accurate throughout the cycle despite the fact that no reversed shear was recorded when it is invariably predicted (cf. § 3.2), is not substantiated by a description of unsteady calibration experiments and must be regarded with some scepticism. We may also note here that the electrochemical technique is even less appropriate than the hot-film for unsteady studies, in models or casts of arteries, since  $\kappa$  is much smaller for electrolytes in water than for heat ( $\kappa \approx 10^{-9} \text{ m}^2 \text{ s}^{-1}$ ), making  $\lambda$  larger.

Further problems in using a hot-film shear probe *in vivo* are the difficulty in setting the film flush with the pulsating vessel wall and the three-dimensional character of flow in most arteries, leading to

two unsteady components of wall shear stress. The former is important because even a slight protrusion into the vessel can seriously disturb the local shear distribution (Lutz *et al.*, 1977). The latter may actually be an advantage because it means that the shear stress *vector* does not fall to zero at most points on the artery wall, so, if the probe is insensitive to direction, it can record the magnitude of the vector at all times in the cycle without the problems associated with flow reversal. This could perhaps be achieved by using a film either of circular or of spiral cross-section, and not placing it on a plane of symmetry of the artery.

We have seen that the frequency response of a wall shear probe is expected to be worse than that of a centre-line- (or average-) velocity probe, while a better frequency response is needed. Thus the most accurate way of obtaining a 'measured' waveform of wall shear, at least in a fairly straight segment of artery far from its entrance, is probably to measure the centre-line velocity and calculate the wall shear from Womersley's equations (3.1*a-d*), since the velocity waveform is known to be related to the pressure gradient as in a rigid tube (fig. 2.5). The improvement in frequency response required of velocity probes is not as dramatic as, and is much more feasible than, that which would be needed from direct wall shear measurement. This method will be inaccurate in arteries so small that the profile in the core is not flat, and near the entrance of an artery where Womersley's theory is invalid (especially for the mean shear: see § 3.2). It will also, of course, be inaccurate near branches and bends.

Ling & Atabek (1972) have proposed that the way to derive a 'measured' waveform of wall shear is to measure the pressures at two nearby stations, calculate the pressure gradient from them, and then use a non-linear theory (based on approximate integration of the axisymmetric equations of motion, including radial wall displacement and fluid viscosity, but not wall viscoelasticity) to compute the velocity and wall shear waveforms. They have used this method in the aorta and in the coronary arteries (Ling *et al.*, 1973; Atabek, Ling & Patel, 1975), and there is no reason to doubt the accuracy of the method. However, there is no evidence that it is more accurate than that proposed above, it requires two simultaneous measurements (of pressure) instead of only one

(of velocity), and the computations would be laborious for a newcomer to the field to reproduce, while use of (3.1*b* and *d*) needs only a standard Fourier-series routine.

The next section and the following two chapters are concerned with the theoretical prediction of wall shear at arterial sites where the above semi-empirical method of determining it cannot be used.

### 3.2 Entry flow in a straight tube

The aorta has been the site of a high proportion of velocity-profile measurements; different parts of the aortic wall also have different mass-transport properties and different susceptibilities to atheroma (§ 1.2); it is therefore a vessel in which prediction of the wall shear, as a function of position and time, is desirable. The geometry of the aorta is complicated, as shown in fig. 1.4, and in order to isolate different effects we make several drastic simplifications. The thoracic aorta is modelled as a uniform, rigid, curved tube of circular cross-section, with a flat, but unsteady, velocity profile entering from the aortic valve. Either the pressure gradient or the centre-line (or average) velocity can be regarded as given, and the neglect of elasticity is justified by the correspondence between rigid-tube theory and experiment (fig. 2.5). Kuchar & Ostrach (1966) calculated entry flow in an elastic tube. They found that elasticity was important only within about one tube radius of the entrance, and depended strongly on the boundary condition that the tube radius was rigidly fixed there. We take the origin  $x = 0$  at the downstream end of the aortic valve, where expansion is possible; thus the tube remains effectively parallel-sided at all times, since the wavelength of the pressure wave greatly exceeds the longitudinal excursion of any fluid element. The gradual taper of the real aorta can be neglected for similar reasons.

The branches from the arch of the aorta will clearly have a significant influence on the flow near their entrances. However, their effect on the flow nearer to the heart is likely to be less pronounced; as we shall see, the skewed velocity profiles in this region of the canine aorta can be accounted for by the curvature of the vessel. The flows in certain types of branch are discussed in chapter 5. The two effects remaining to be analysed are those of

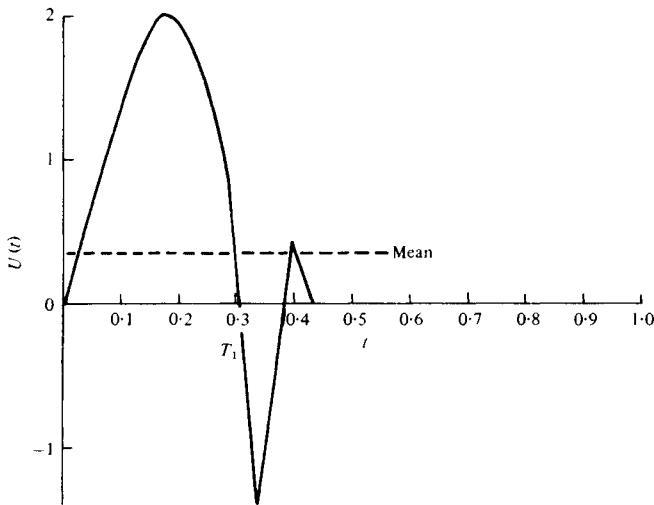


Fig. 3.3. Dimensionless velocity,  $U(t)$ , in the core of the aorta, simplified from a measured waveform presented by Nerem *et al.* (1972). Peak velocity ( $U = 2$ ) is  $1 \text{ m s}^{-1}$ , mean velocity ( $U = 0.34$ ) is  $0.17 \text{ m s}^{-1}$ ; duration of beat ( $t = 1$ ) is  $0.4 \text{ s}$ . (After Pedley, 1976a.)

unsteadiness and of curvature. Curvature is discussed in the next chapter; in this section we simplify the problem still further and consider unsteadiness alone, analysing unsteady entry flow in a straight tube. The incoming waveform of centre-line velocity is taken to have a shape typical of that measured in the canine ascending aorta, as shown in fig. 1.14(b) and modelled in fig. 3.3, where the peak velocity is  $1 \text{ m s}^{-1}$ , where there is flow reversal with a maximum negative velocity of  $-0.7 \text{ m s}^{-1}$ , and where the mean velocity is  $0.17 \text{ m s}^{-1}$  (Nerem, *et al.*, 1972). Note that the neglect of curvature is partly justified by the fact that the initial part of the ascending aorta is more or less straight, curvature developing only after 2 or 3 cm.

### 3.2.1 Steady flow

Steady axisymmetric entry flow in a tube, with a more or less flat velocity profile at  $x = 0$ , has been the subject of theoretical study for many years (see Goldstein, 1938; Schlichting, 1968). In the limit of large Reynolds number  $Re (= 2Ua/\nu)$ , where  $a$  is tube radius and  $U$

is the average fluid velocity), the flow can be divided into three regions, excluding a small region of length-scale  $\nu/U$  near the rim of the tube entrance at  $x = 0$ .

(a) For  $x/a = O(1)$ , a boundary layer on the wall  $r = a$ , of thickness  $\delta \propto (\nu x/U)^{1/2}$ , in which the longitudinal velocity profile is that of a Blasius boundary layer to leading order, with a correction of  $O(Re^{-1/2})$ :

$$u = U[f'_0(\eta) + O(Re^{-1/2})], \quad (3.6)$$

where  $\eta = y(U/2\nu x)^{1/2}$ ,  $y = a - r$ , and  $f_0(\eta)$  is the Blasius function.

(b) Also for  $x/a = O(1)$ , there is an inviscid core, consisting of a uniform velocity plus a correction due to the displacement effect of the Blasius boundary layer (Van Dyke, 1970; Wilson, 1971); for the case when the entry condition is that of irrotational, but not necessarily exactly parallel, flow ( $u = U$ ,  $\partial v/\partial x = 0$ , where  $v$  is the radial velocity component), the axial velocity profile in the core is

$$\frac{u}{U} = 1 + \frac{\beta_0}{(\pi Re)^{1/2}} \int_0^\infty \frac{\sigma^{-1/2} I_0(\sigma r/a)}{I_1(\sigma)} \sin(\sigma x/a) d\sigma + O(Re^{-1}),$$

where  $\beta_0 = \lim_{\eta \rightarrow \infty} (\eta - f_0) \approx 1.217$  (Singh, 1974). The  $O(Re^{-1/2})$  correction to the core flow satisfies the boundary condition

$$v/U \sim -\beta_0/(2Re x/a)^{1/2} \quad \text{at } r = a,$$

and as  $x/a \rightarrow \infty$  the axial velocity component has the asymptotic expansion

$$\frac{u}{U} \sim 1 + \frac{2\beta_0}{Re^{1/2}} \left[ \left( \frac{2x}{a} \right)^{1/2} + O\left( \frac{x}{a} \right)^{-1/2} \right] + o(Re^{-1}),$$

representing a flat profile. Thus the expansion breaks down when  $x/a = O(Re)$  at which point the boundary layers fill the tube ( $\delta = O(a)$ ).

(c) There is therefore a third region, in which  $\xi = x/aRe = O(1)$ , where the boundary layer equations apply (to leading order) for all  $r$ , and the flow develops from a flat core surrounded by a Blasius boundary layer at  $\xi \ll 1$  to Poiseuille flow as  $\xi \rightarrow \infty$ . This development has been calculated numerically (at least for two-dimensional flow) by Bodoia & Osterle (1961).

Despite the displacement effect, and the non-uniform core profile at finite values of  $Re$ , the velocity profile near the wall, and in

particular the wall shear, in the region  $x/a \ll Re$  is given by the Blasius profile (3.6). This means that the boundary layer is so thin that it behaves, to leading order in  $Re^{-1/2}$ , as if it were on a flat plate and not in a tube: the curvature of the walls is irrelevant. We assume that this is also the case in unsteady entry flow, and calculate the structure of the unsteady boundary layer on a semi-infinite flat plate; the procedure is expected to be valid for  $x/a$  much smaller than the mean Reynolds number.

### 3.2.2 Non-reversing unsteady flow

We consider a flat plate occupying the half-plane  $\hat{y} = 0$ ,  $\hat{x} > 0$  (where a hat over a variable means that it is dimensional; this convention will be used from now on), with a viscous incompressible fluid flowing over it in the  $\hat{x}$ -direction. The velocity far from the plate is  $\hat{U}(\hat{t})$ . Suppose that a velocity-scale is  $U_0$  and a time-scale is  $\Omega^{-1}$ , and introduce dimensionless variables,

$$\left. \begin{aligned} x &= \hat{x}\Omega/U_0, & y &= \hat{y}(\Omega/\nu)^{1/2}, & t &= \Omega\hat{t}, & U(t) &= \hat{U}(\hat{t})/U_0, \\ u &= \hat{u}/U_0, & v &= \hat{v}/(\Omega\nu)^{1/2}, & \psi &= (\hat{\psi}/U_0)(\Omega/\nu)^{1/2}, \end{aligned} \right\} \quad (3.7)$$

where  $\hat{u}$ ,  $\hat{v}$ ,  $\hat{\psi}$  are the  $\hat{x}$ - and  $\hat{y}$ -components of velocity, and the stream function, respectively. The velocity field is related to  $\psi$  by

$$(u, v) = (\psi_y, -\psi_x).$$

Boundary layer theory is applicable as long as the Reynolds number,  $U_0^2/\Omega\nu$ , is much greater than 1. The boundary layer equations reduce to

$$\psi_{y,t} + \psi_y\psi_{xy} - \psi_x\psi_{yy} = U_t + \psi_{yyy}, \quad (3.8)$$

which is to be solved subject to boundary conditions:

$$\left. \begin{aligned} \psi &= \psi_y = 0 && \text{on } y = 0 \text{ (no slip)} \\ \psi_y &\sim U(t) && \text{as } y \rightarrow \infty. \end{aligned} \right\} \quad (3.9)$$

The function  $U(t)$  should eventually be taken to be of the form shown in fig. 3.3; however, this subsection is devoted to non-reversing flow, and when it is necessary to specify  $U(t)$ , we take as a prototype

$$U(t) = 1 + \alpha \sin t, \quad (3.10)$$

where the amplitude parameter,  $\alpha$ , is less than 1.

This problem has been investigated by several authors. The best known early work is that of Lighthill (1954), who restricted himself to  $\alpha \ll 1$ , and used a Karman-Pohlhausen method to compute the skin friction for both large and small values of  $x$ . Moore (1951, 1957) showed that the small- $\alpha$  restriction is unnecessary for the small- $x$  expansion, and Lin's (1956) expansion for large  $x$  did not require the restriction either. This seems not to have been generally realised, however, until Pedley (1972*b*) combined the two approaches, and extended them to cover a free stream whose velocity varies as a power of  $x$ . The following account is a summary of the large-amplitude theory for the flat plate; its object is to calculate the dimensionless wall shear stress

$$S(x, t) = \psi_{yy}|_{y=0}$$

for all  $t$  and for as wide a range of values of  $x$  as possible.

### *Small $x$*

At a fixed value of  $\hat{x}$  we would expect the flow to be a quasi-steady Blasius boundary layer if the frequency  $\Omega$  is low enough. This suggests that an expansion in powers of the dimensionless coordinate  $x$  should have the quasi-steady solution as its first term. We therefore introduce appropriate similarity variables,  $\eta_1$  and  $\phi$ , such that

$$y = [2x/U(t)]^{1/2} \eta_1, \quad \psi = [2xU(t)]^{1/2} \phi,$$

and the governing equation, (3.8), becomes

$$\phi_{\eta_1 \eta_1 \eta_1} + \phi \phi_{\eta_1 \eta_1} + 2x[\phi_x \phi_{\eta_1 \eta_1} - \phi_{\eta_1} \phi_{x \eta_1} + (\dot{U}/U^2)(1 - \phi_{\eta_1} - \frac{1}{2} \eta_1 \phi_{\eta_1 \eta_1}) - (1/U) \phi_{\eta_1 t}] = 0. \quad (3.11)$$

The boundary conditions are

$$\phi = \phi_{\eta_1} = 0 \quad \text{on} \quad \eta_1 = 0, \quad \phi_{\eta_1} \rightarrow 1 \quad (\text{exponentially}) \quad \text{as} \quad \eta_1 \rightarrow \infty.$$

Formally putting  $x = 0$ , we see that the problem reduces to that of the Blasius boundary layer, with solution  $\phi = f_0(\eta_1)$ . We therefore seek a solution in powers of  $x$ :

$$\phi = f_0(\eta_1) + \sum_{m=1}^{\infty} x^m \phi_m(\eta_1, t), \quad (3.12)$$

where the functions  $\phi_m$  satisfy homogeneous boundary conditions in  $\eta_1$ , but inhomogeneous differential equations. Substitution into (3.11) and equating first and second powers of  $x$  show that

$$\phi_1 = \frac{\dot{U}}{U^2} f_{11}(\eta_1), \quad \phi_2 = \frac{\dot{U}^2}{U^4} f_{21}(\eta_1) + \frac{\ddot{U}}{U^3} f_{22}(\eta_1),$$

where  $f_{mk}(\eta_1)$  satisfies the ordinary differential equation

$$f_{mk}''' + f_0 f_{mk}'' - 2m f_0' f_{mk}' + (2m+1) f_0'' f_{mk} = \mathcal{F}_{mk}(\eta_1) \quad (3.13)$$

and

$$\mathcal{F}_{11} \equiv \eta_1 f_0'' + 2(f_0' - 1), \quad \mathcal{F}_{22} \equiv 2f_{11}',$$

$$\mathcal{F}_{21} \equiv 2f_{11}'^2 - 3f_{11} f_{11}'' + \eta_1 f_{11}'' - 2f_{11}'.$$

These equations have been solved numerically, and the values of  $f_{mk}''(0)$  and of  $\beta_{mk} \equiv \lim_{\eta_1 \rightarrow \infty} (-f_{mk})$  are given in table 3.1. The dimensionless skin friction is

$$S = \frac{U^{3/2}(t)}{(2x)^{1/2}} \left\{ f_0''(0) + \frac{x\dot{U}}{U^2} f_{11}''(0) + x^2 \left[ \frac{\dot{U}^2}{U^4} f_{21}''(0) + \frac{\ddot{U}}{U^3} f_{22}''(0) \right] + O(x^3) \right\}. \quad (3.14)$$

Another quantity that proves to be of importance is the displacement thickness  $\hat{\delta}_1$  defined by

$$\hat{\delta}_1 = \int_0^\infty \left( 1 - \frac{\hat{u}}{\hat{U}} \right) d\hat{y},$$

Table 3.1. *Values of  $f_{mk}''(0)$  and of  $\beta_{mk} = \lim_{\eta_1 \rightarrow \infty} (-f_{mk})$ , ( $f_{00} \equiv f_0 - \eta$ )*

$m$	$k$	$f_{mk}''(0)$	$\beta_{mk}$
0	0	0.470	1.217
1	1	1.200	-0.727
2	1	0.383	-0.541
2	2	-0.664	0.845



so that the dimensionless displacement thickness  $\delta_1 = (\Omega/\nu)^{1/2} \hat{\delta}_1$  is equal to

$$\delta_1 = \left(\frac{2x}{U}\right)^{1/2} \left[ \beta_0 + \frac{x\dot{U}}{U^2} \beta_{11} + x^2 \left( \frac{\dot{U}^2}{U^4} \beta_{21} + \frac{\ddot{U}}{U^3} \beta_{22} \right) + O(x^3) \right]. \quad (3.15)$$

The above expansion shows that the quasi-steady solution is accurate at a given value of  $x$  as long as

$$\varepsilon = |x\dot{U}/U^2| \quad (3.16)$$

is much less than 1 for all  $t$ . The series itself will be a useful asymptotic expansion if  $\varepsilon$  (and  $|x^2\ddot{U}/U^3|$ ) is small enough for the  $O(x^2)$  term to be small compared with the  $O(x)$  term for all  $t$ . In that case the first two terms will be a reasonable approximation to the almost quasi-steady solution. Pedley (1972*b*) made a number of computations, and a useful rule of thumb to emerge is that the first two terms are quite accurate as long as  $\varepsilon < 0.5$ . An example is given in fig. 3.4, where the values of  $S$  calculated from one, two and three terms of (3.14) are plotted against  $t$  for the case when  $U$  is sinusoidal, given by (3.10) with  $\alpha = 0.5$ , and  $x = 0.6$ . The three-

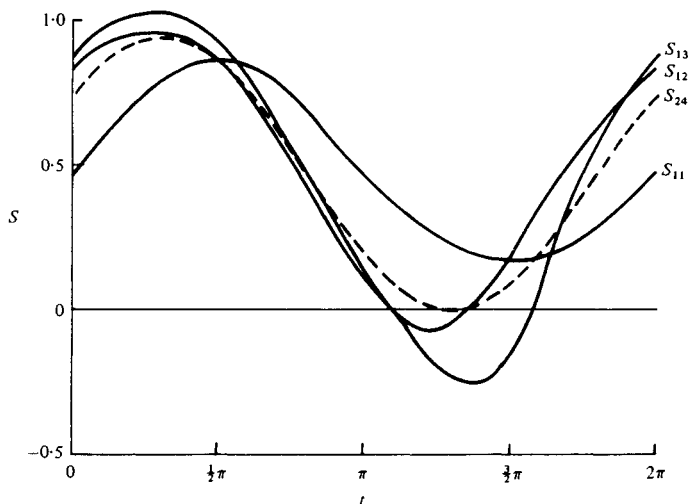


Fig. 3.4. Graphs of  $S$  against  $t$  as calculated from one, two and three terms of (3.14) (continuous curves,  $S_{11}$ ,  $S_{12}$ ,  $S_{13}$ ) and as calculated from (3.30) with  $\gamma = 0$  (broken curve,  $S_{24}$ ).  $\alpha = 0.5$ ,  $x = 0.6$ . (After Pedley, 1972*b*.)

term expansion differs significantly from the two-term expansion (and both are therefore inaccurate) for  $t$  between about  $\frac{5}{4}\pi$  and  $\frac{7}{4}\pi$ , at which times  $\varepsilon = 0.51$ . Note, incidentally, that although the free stream does not reverse its direction, the shear at the wall is predicted to do so in the example shown. This is because the slowly moving fluid near the wall, with little inertia, tends to respond instantaneously to the pressure gradient  $U_n$ , which is negative for half the cycle. This also accounts for the phase lead of the actual wall shear over the free-stream velocity (i.e. over the quasi-steady wall shear).

### *Large $x$*

If the flow were purely oscillatory, so that for large  $x$  the influence of the leading edge could not be felt, we would expect the flow to be that of the classical Stokes oscillatory boundary layer. This is the solution of (3.8) and (3.9) that is independent of  $x$ ; the departure from the free stream would be confined to a boundary layer of (non-dimensional) thickness 1. On the other hand, if the amplitude of the oscillations in the free stream were very small compared with the mean velocity ( $\alpha \ll 1$  in (3.10)), the flow should be approximately given by the Blasius boundary layer, with thickness  $(2x)^{1/2}$ . This suggests that for large  $x$  (when  $(2x)^{1/2} \gg 1$ ) there are two length-scales for variation in the  $y$ -direction, one primarily associated with the mean flow and one with the oscillations. Together with the observation that the coefficient of the highest-order derivative ( $\phi_{\eta_1\eta_1\eta_1}$ ) in (3.11) is small compared with that of other terms, this makes it clear that a solution should be sought by the method of matched asymptotic expansions (Van Dyke, 1975). We introduce outer and inner variables as follows:

Outer:

$$\eta = y/(2x)^{1/2}, \quad \tilde{\psi} = (2x)^{-1/2}\psi,$$

Inner:

$$\zeta = y/\sqrt{2} = x^{1/2}\eta, \quad \Psi = \psi/\sqrt{2} = x^{1/2}\tilde{\psi},$$

where the  $\sqrt{2}$  is retained in the inner variables so that they are the same as those used by Pedley (1972*b*). From now on  $U(t)$  is restricted for convenience to take the form (3.10).

*Outer expansion.* In terms of the outer variables, (3.8) becomes

$$2\tilde{\psi}_{\eta t} - (1/x)[\tilde{\psi}_{\eta\eta\eta} + \tilde{\psi}\tilde{\psi}_{\eta\eta} + 2x(\tilde{\psi}_x\tilde{\psi}_{\eta\eta} - \tilde{\psi}_{x\eta}\tilde{\psi}_\eta)] = 2\alpha \cos t. \quad (3.17)$$

The outer boundary condition is that

$$\psi_\eta \rightarrow 1 + \alpha \sin t \quad \text{as } \eta \rightarrow \infty, \quad (3.18)$$

while the inner condition is that of matching to the inner solution. We would also like to impose the condition that, as  $\alpha \rightarrow 0$ ,  $\tilde{\psi}$  takes its steady form  $f_0(\eta)$ . We seek an expansion for  $\tilde{\psi}$  of the form

$$\tilde{\psi} = \sum_{m=0}^{\infty} x^{-m/2} \tilde{\psi}_m(\eta, t),$$

and substitute it into (3.17), equating like powers of  $x$ , to obtain a series of equations for  $\tilde{\psi}_m$ . The zeroth-order equation is

$$\tilde{\psi}_{0\eta t} = \alpha \cos t,$$

and the general solution satisfying (3.18) is

$$\tilde{\psi}_0 = \alpha \eta \sin t + f_0(\eta) + \dot{T}_0(t), \quad (3.19)$$

where the last two terms tend to zero as  $\alpha \rightarrow 0$  but are otherwise arbitrary functions.  $\dot{T}_0$  is expected to be oscillatory with zero mean; any constant part can be incorporated into  $F_0$ . The solution of the first order equation is

$$\tilde{\psi}_1 = F_1(\eta) + \dot{T}_1(t), \quad (3.20)$$

where  $F_1$  and  $\dot{T}_1$  are arbitrary (a dot and a prime denote differentiation with respect to  $t$  and  $\eta$  respectively). The equation for  $\tilde{\psi}_2$  is

$$2\tilde{\psi}_{2\eta t} = \bar{f}_0''' + (\eta\alpha \sin t + \bar{f}_0' + \dot{T}_0)\bar{f}_0'', \quad (3.21)$$

where (3.19) has been used, with  $\bar{f}_0 \equiv f_0 + F_0$ . In order that there should be no secular terms,  $\bar{f}_0(\eta)$  must satisfy the same equation as the Blasius function  $f_0$ , which also satisfies both the wall boundary conditions and the steady part of the outer boundary condition, but we cannot yet rule out the existence of functions  $F_0(\eta)$  such that  $F_0(0)$  or  $F_0'(0)$  is non-zero. After the time-independent part of (3.21) is removed, that equation can be integrated to give

$$\tilde{\psi}_2 = -\frac{1}{2}\alpha \cos t (\eta \bar{f}_0' - \bar{f}_0) + \frac{1}{2} \bar{f}_0' T_0(t) + F_2(\eta) + \dot{T}_2(t), \quad (3.22)$$

where again the last two terms are arbitrary. In all cases we expect

the arbitrary functions occurring in  $\tilde{\psi}_m$  to be determined by the equation obtained from prohibiting secular terms in  $\tilde{\psi}_{m+2}$  and by boundary conditions derived from the inner expansion. Eigenfunctions may occur (solutions that satisfy both the outer and the wall boundary conditions identically), and they cannot be determined without taking into account conditions at the leading edge (see p. 147).

The problems for  $\tilde{\psi}_3$  and  $\tilde{\psi}_4$  can be solved similarly. For secular terms to be absent,  $F_1(\eta)$  and  $F_2(\eta)$  must satisfy the equations

$$F_m''' + \bar{f}_0 F_m'' + m \bar{f}_0' F_m' + (1-m) \bar{f}_0'' F_m = -\delta_{m2} F_1'^2 \quad (m = 1, 2) \quad (3.23)$$

and  $F_m'$  should tend to zero as  $\eta_1 \rightarrow \infty$ . The solution for  $\tilde{\psi}_3$  is

$$\tilde{\psi}_3 = -\frac{1}{2}[\alpha \eta \cos t - T_0(t)]F_1' + F_3(\eta_1) + \dot{T}_3(t), \quad (3.24)$$

while that for  $\tilde{\psi}_4$  is

$$\begin{aligned} \tilde{\psi}_4 = & -\frac{1}{4}\alpha \bar{\alpha}_2 \sin t \\ & + \frac{1}{16}\alpha^2 \cos 2t (\eta^2 \bar{f}_0'' + \eta \bar{f}_0' - \bar{f}_0) \\ & - \frac{1}{2}\alpha \cos t (\eta F_2' + F_2) - \frac{1}{2}T_2(t) \bar{f}_0' + F_4(\eta) + \dot{T}_4(t), \end{aligned} \quad (3.25)$$

where  $\bar{\alpha}_2 = \bar{f}_0''(0)$  and a number of terms containing  $T_0(t)$  have been omitted because that function is subsequently shown to be zero. In each case the last two terms are arbitrary functions. The outer boundary conditions on the terms in the inner expansion are obtained by rewriting the outer expansion in terms of the inner variable  $\zeta = x^{1/2}\eta$  and expanding in powers of  $x^{-1/2}$ . Each term of that expansion can be used as the large- $\zeta$  condition on a corresponding term of the inner solution.

*Inner expansion.* In terms of inner variables, (3.8) is unchanged, as follows:

$$2\Psi_{\zeta t} - \Psi_{\zeta\zeta\zeta} + 2(\Psi_{x\zeta}\Psi_{\zeta} - \Psi_x\Psi_{\zeta\zeta}) = 2\alpha \cos t,$$

with inner boundary condition

$$\Psi = \Psi_{\zeta} = 0 \quad \text{at } \zeta = 0;$$

we seek a solution of the form

$$\Psi = \sum_{m=-1}^{\infty} x^{-m/2} \Psi_m(\zeta, t).$$

The problem for  $\Psi_{-1}$  is then

$$2\Psi_{-1\zeta t} - \Psi_{-1\zeta\zeta\zeta} = 0;$$

$$\Psi_{-1}(0, t) = \Psi_{-1\zeta}(0, t) = 0, \quad \Psi_{-1}(\infty, t) = F_0(0) + \dot{T}_0(t),$$

which has no steady or periodic (non-diffusing) solution unless  $\Psi_{-1}(\infty, t) = 0$ , when  $\Psi_{-1} \equiv 0$ . Thus  $T_0(t) \equiv 0$ ,  $F_0(0) = 0$ . The problem for  $\Psi_0$  is

$$2\Psi_{0\zeta t} - \Psi_{0\zeta\zeta\zeta} = 2\alpha \cos t,$$

with outer boundary condition

$$\Psi_0(\infty, t) \sim F_1(0) + \dot{T}_1(t) + \alpha\zeta \sin t + \zeta F'_0(0),$$

from (3.19) and (3.20). This has no periodic solution unless

$$F'_0(0) = F_1(0) = 0, \quad T_1(t) = \frac{1}{2}\alpha(\sin t + \cos t), \quad (3.26)$$

and then

$$\Psi_0 = \alpha\zeta \sin t - \text{Im} \left\{ \frac{\alpha e^{it}}{1+i} [1 - e^{-(1+i)\zeta}] \right\}. \quad (3.27)$$

This represents the Stokes layer, and has zero mean. Furthermore, we now have three, homogeneous, boundary conditions on  $F_0(\eta)$ , which is therefore identically zero since  $f_0(\eta)$  is the unique solution of the equation and boundary conditions defining the Blasius function (Coppel, 1960). Hence the leading term in the inner expansion is the *oscillatory* Stokes layer, with no contribution from the mean flow, while the leading term in the outer expansion is the *steady* Blasius boundary layer corresponding to the mean velocity, plus the inviscid oscillations of the free stream (the term  $\alpha\eta \sin t$  in (3.19)). To leading order in  $x^{-1/2}$ , therefore, the mean and oscillatory components of the flow are completely uncoupled and do not interact.

Subsequent terms in the inner expansion, and boundary conditions on the unknown terms of the outer expansion, are obtained similarly. We require the expansion

$$f_0(\eta) = \frac{1}{2}\alpha_2\eta^2 - (\alpha_2^2/5!)\eta^5 + O(\eta^8),$$

where  $\alpha_2 = f''_0(0)$  is given in table 3.1. The results for the next three terms are given below. First

$$\Psi_1 = \frac{1}{2}\alpha_2\zeta^2, \quad (3.28)$$

the innermost part of the steady Blasius layer, requiring

$$F'_1(0) = F_2(0) = T_2(t) = 0.$$

Then

$$\Psi_2 = \frac{1}{2} F_1''(0) \zeta^2,$$

requiring

$$F_3(0) = F_2'(0) = T_3(t) = 0.$$

Finally

$$\begin{aligned} \Psi_3 = & \frac{1}{2} F_2''(0) \zeta^2 + \text{Im} \{ \alpha \alpha_2 e^{i\tau [\frac{13}{32} - \frac{1}{4}i\zeta^2} \\ & - e^{-k\tau (\frac{13}{32} + \frac{13}{32}k\zeta + \frac{5}{16}i\zeta^2 - \frac{1}{24}\bar{k}\zeta^3)} \} \}, \end{aligned} \quad (3.29)$$

where  $k = 1 + i$ ,  $\bar{k} = 1 - i$ , and we require

$$F_3'(0) = F_4(0) = 0, \quad T_4(t) = -\frac{21}{32} \alpha \alpha_2 \cos t.$$

This last term is the first in which interaction between the oscillatory flow and the mean becomes apparent, through both  $\Psi_3$  and  $T_4(t)$ .

Note that all the boundary conditions for the functions  $F_1$ ,  $F_2$  and  $F_3$  have now been obtained. Unless there is an eigensolution, they will all be identically zero. It is a simple matter to show that  $F_1$  and  $F_3$  are identically zero, but the problem for  $F_2$  is satisfied by an arbitrary multiple of  $\eta f_0' - f_0$  (Stewartson, 1957; Libby & Fox, 1963). The appearance of eigenfunctions is to be expected on physical grounds because the large- $x$  expansion must in some way be influenced by different conditions near the leading edge. The eigensolutions that emerge in the above way are also eigensolutions of the steady boundary layer equations; unsteadiness could come in only at subsequent terms in the expansion where  $F_2(\eta)$ , say, may be multiplied by functions of time. The above procedure also yields only those eigensolutions that correspond to integer powers,  $m$ , of  $x^{-1/2}$ , whereas all powers will in general be required to take account of upstream conditions. However, Libby & Fox (1963) showed numerically that  $m = 2$  is the first eigenvalue, and that the second is  $m = 3.77$ ; the above expansion was therefore terminated at  $m = 3$ .

There is also the possibility of eigensolutions that are intrinsically unsteady. Brown & Stewartson (1973) have investigated these, and found a class of very complicated eigensolutions, whose structure suggests that disturbances are propagated downstream near the edge of the Blasius boundary layer with approximately the free-stream velocity, and their effect then diffuses both inwards to the wall and out into the free stream. At any given time, the variation

with  $x$  of the disturbance to the boundary layer has the form of a decaying oscillation, which was also found in a numerical solution to the small-amplitude equations by Ackerberg & Phillips (1972). Both groups emphasised the marked influence of these eigen-solutions on the unsteady displacement thickness of the boundary layer, while the influence on the wall shear is small since the eigensolutions are greatest at the edge of the boundary layer.

If we ignore this class of eigensolutions, we may write down the large- $x$  expansion for the dimensionless wall shear,  $S$ :

$$S = \frac{1}{\sqrt{2}} \Psi_{\zeta\zeta} \Big|_{\zeta=0} = (\alpha/\sqrt{2})(\cos t + \sin t) + (2x)^{-1/2} \alpha_2 + (x^{-3/2}/\sqrt{2}) \gamma \alpha_2 - \frac{5}{16} \alpha \alpha_2 \cos t + O(x^{-2}). \quad (3.30)$$

The large- $x$  expansion for the dimensionless displacement thickness, again ignoring the eigensolutions other than  $F_2(\eta)$ , is

$$\delta_1 = (2x)^{1/2}/(1 + \alpha \sin t) [\beta_0 - (\alpha/2x^{1/2})(\cos t - \sin t) + (\beta_0/x)(\frac{1}{2}\alpha \cos t - \gamma) + O(x^{-2})]; \quad (3.31)$$

in both these equations  $\gamma$  is defined by

$$F_2(\eta) = \gamma(\eta f'_0 - f_0).$$

*Matching.* Pedley (1972*b*), reviewing the numerical results of a number of papers, showed that the amplitudes and phases of the wall shear oscillations calculated from the small- and large- $x$  expansions, (3.14) and (3.30), are close together for  $x$  in the range 0.5–0.7 for several values of  $\alpha$  up to 0.8. Agreement was closer when only two terms of (3.14) were used than when three terms were used, presumably because at this value of  $x$  there is a range of values of  $t$  for which  $\varepsilon = |x\dot{U}/U^2|$  exceeds 0.5. Fig. 3.4 shows the close correspondence between the wall shear calculated from (3.30) and that from two terms of (3.14) when  $x = 0.6$  and  $\alpha = 0.5$ . In the large- $x$  expansion, Pedley arbitrarily took  $\gamma = 0$ , and fig. 3.4 indicates that no significant improvement can be expected by choosing any other value for  $\gamma$ , which would merely alter the mean shear slightly (see (3.30)): the means with  $\gamma = 0$  differ only because the mean value of  $(1 + \alpha \sin t)^{3/2}$  is not precisely 1. Similar

conclusions are reached if we match the means of the two expansions of the displacement thickness ((3.31) with  $\gamma = 0$  and two terms of (3.15)).

The expansion (3.30) shows that the phase lead of the shear over the free stream tends to the limit  $\frac{1}{4}\pi$  as  $x \rightarrow \infty$ . In fact, if we write

$$S = \bar{S} + \alpha S_1 \sin(t + \frac{1}{4}\pi - \chi),$$

where  $\bar{S}$  is the mean shear and  $\frac{1}{4}\pi - \chi$  is the phase lead, we obtain

$$\chi \approx 1 - S_1 \approx 0.073x^{-3/2}.$$

This indicates that the asymptotic limit, in which the mean flow is uncoupled from the oscillation, is accurate to within 10% for  $x$  as low as 0.81.

Finally, we may notice that the large- $x$  expansion does not formally require the restriction that  $\alpha < 1$ , i.e. that the free stream is non-reversing. Thus, where the influence of the leading edge is manifest only in the development of the mean flow, the amplitude of the oscillation can be as large as we please, although the small- $x$  expansion is clearly not valid throughout the cycle in a reversing flow, because  $\varepsilon$  becomes infinite when  $U$  passes through zero.

### 3.2.3 Reversing flow

The aim of this subsection is to investigate the flow near the leading edge of a semi-infinite flat plate (i.e. the entry flow in a tube) when the free stream reverses its direction. The work described is largely contained in the paper by Pedley (1976*a*). We shall consider a free stream whose velocity varies with time like that shown in fig. 3.3. Since this represents a periodic motion, we expect that far from the leading edge the whole flow can be described as a developing mean flow superimposed on a number of oscillatory terms, each representing the Stokes layer corresponding to one Fourier component of the waveform. From the work described above, this is expected to be valid for dimensional distances  $\hat{x}$  greater than approximately  $1.0 U_0/\Omega$ , where  $U_0$  is the mean velocity, and  $\Omega$  is the lowest angular frequency of the motion. In the example shown in fig. 3.3, this distance is only about 1.1 cm, but, as we shall see, the large amplitude of the oscillations means that the influence of the



leading edge (other than in the development of the mean flow) is felt up to  $\hat{x} = 4\text{--}5$  cm at some stage during the cycle.

The main additional assumption to be made is that the flow in the aorta (or over the flat plate) comes completely to rest at the end of each cycle. This is based on the fact that the free-stream velocity (fig. 3.3) is zero for more than half the cycle; but it cannot be strictly true since there will inevitably be residual motions in the boundary layer when the free stream has come to rest, and these will take a time proportional to  $a^2/\nu$  to decay (here  $a$  is the radius of the aorta, so the decay time is about 20 s). However, these residual motions turn out to be very small, and it is consistent to neglect them in describing the large oscillatory wall shear during systole. This assumption is very useful, because it means that the thickness of the boundary layer that develops on the tube wall during every beat never exceeds a value proportional to  $(\nu T)^{1/2}$ , where  $T$  is the period of the beat. For blood in the dog aorta,  $(\nu T)^{1/2} \approx 0.13$  cm, which is less than a tenth of the vessel diameter. Therefore we are still justified in neglecting the curvature of the tube wall.

The development with time of the flow at a given value of  $\hat{x}$  quite near the leading edge can be described qualitatively as follows. Initially vorticity diffuses out from the wall in a time-dependent but  $\hat{x}$ -independent manner, and is restricted to a Rayleigh layer of thickness proportional to  $(\nu t)^{1/2}$ . This persists until fluid particles that have passed the leading edge arrive at  $\hat{x}$ ; from then on the diffusive flow is continuously modified until eventually an approximately quasi-steady boundary layer is set up, described by the first one or two terms of the expansion (3.12). This modification is quite rapid in the case of the impulsively started flat plate (Hall, 1969), and we may suppose that it is quite rapid in the present case too. The approximately quasi-steady boundary layer is expected to persist until after the peak velocity has passed, but must break down again well before the free-stream velocity becomes zero. Near the time of zero velocity the convective inertia terms will be small, and the flow is expected once more to represent a diffusive balance between unsteady inertia and viscosity. Subsequent oscillations could be treated similarly, but it turns out that for values of  $\hat{x}$  that are of interest the influence of the leading edge is not felt after the first reversal, and the flow remains diffusive until the next cycle. The

main approximation of the theory to be outlined here is to treat the transitions between diffusive and approximately quasi-steady flows as instantaneous, not gradual.

The variables are non-dimensionalised as in (3.7), with  $\Omega$  replaced by  $1/T$ , where  $T$  is the period of the cycle. The boundary layer equation for the longitudinal velocity  $u$ , (3.8), can be written as

$$(u_t - U_t) + \left( uu_x - u_y \int_0^y u_x \, dy \right) = u_{yy}, \quad (3.32)$$

with boundary and initial conditions  $u = 0$  on  $y = 0$ ,  $u \rightarrow U(t)$  as  $y \rightarrow \infty$ , and  $u = 0$  at  $t = 0$ . We assert that the initial diffusive solution, a balance between the first term in brackets on the left-hand side of (3.32) and the viscous term on the right-hand side, holds exactly until a certain time,  $t'_1(x)$ , which is to be determined (it will be the time at which the influence of the leading edge is first felt at  $x$ ). That is,

$$u = U(t) - 2\pi^{-1/2} \int_{\eta_0}^{\infty} U \left[ t - \frac{\eta_0^2(t-t'_0)}{\mu^2} \right] e^{-\mu^2} d\mu \quad \text{for } 0 < t \leq t'_1(x), \quad (3.33)$$

where

$$\eta_0 = \frac{1}{2}y(t-t'_0)^{-1/2}$$

and the time origin of the diffusion is  $t'_0 = 0$ . After this time, we assert that there is a sudden transition to the approximately quasi-steady solution represented by (3.12) which holds until another transition time  $t'_2(x)$ ; that is,

$$u = U(t)[f'_0(\eta_1) + (x\dot{U}/U^2)f'_{11}(\eta_1)] \quad \text{for } t'_1(x) < t < t'_2(x) \quad (3.34)$$

where  $\eta_1 = y[U(t)/2x]^{1/2}$ ,  $f_0$  is the Blasius function and  $f_{11}$  is the solution of (3.13) with  $m = k = 1$ . (The primes on the times  $t'_0$ ,  $t'_1$ ,  $t'_2$  are put there because these are not the same as the times  $t_0$ ,  $t_1$ ,  $t_2$  defined by Pedley (1976a).) The expansion (3.34) in no way takes account of the flow before  $t = t'_1(x)$ , so there will inevitably be a discontinuity at that time; the removal of that discontinuity involves an extremely complicated exercise in multi-layered boundary layer theory, even in the apparently simple case of the impulsively started flat plate (Stewartson, 1973), and will not be attempted here. As in

the case of the periodic boundary layer considered above, the influence of the leading edge is convected along the outer edge of the boundary layer, at approximately the free-stream velocity, and its effect then diffuses into the inner parts of the layer, affecting the wall shear somewhat later than, say, the displacement thickness.

A new diffusive flow takes over from the quasi-steady flow at  $t = t'_2(x)$ , and persists until the end of the cycle,  $t = 1$ . This will again represent a solution of (3.32) without the convective inertia terms, which should be solved subject to an initial condition derived from (3.34). However, such a solution would be rather cumbersome, and we make the further approximation that the new diffusive solution also takes the form (3.33), with the disposable function  $t'_0(x)$  chosen to make the displacement thickness of the boundary layer continuous at  $t = t'_2$ . The displacement thickness is chosen because it is thought to be the most fundamental single parameter representing the motion in a boundary layer (in any case, choosing another parameter, such as momentum thickness, makes little difference to the results (Pedley, 1976a)). Continuity of displacement thickness (see (3.15)) at  $t = t'_2$  requires that

$$[2xU(t'_2)]^{1/2} \left[ \beta_0 + \frac{x\dot{U}(t'_2)}{U^2(t'_2)} \beta_{11} \right] \\ = 2 \left( \frac{t'_2 - t'_0}{\pi} \right)^{1/2} \int_0^1 U[t'_2 - \lambda^2(t'_2 - t'_0)] d\lambda, \quad (3.35)$$

where  $\beta_0 (= \beta_{00})$  and  $\beta_{11}$  are given in table 3.1.

It still remains to determine the take-over times  $t'_1(x)$  and  $t'_2(x)$ . In Pedley (1976a) the former was chosen to be the time at which information about the leading edge is first convected to  $x$  at the edge of the boundary layer, i.e.  $t'_1$  is chosen so that

$$x = \int_0^{t'_1} U(t) dt, \quad (3.36a)$$

although it is recognised that the effect on wall shear is not felt until a little later (Hall, 1969; Dennis, 1972). The second take-over time

is chosen in a similar way:

$$x = \int_{t'_2}^{T_1} U(t) dt, \quad (3.36b)$$

where  $T_1$  is the first zero of  $U(t)$  ( $\approx 0.3$  in fig. 3.3). This means that a fluid particle passing the leading edge at  $t'_2$  only just reaches  $x$  before being swept back by the reversed flow; this seems a reasonable choice, by symmetry with (3.36a), but there is no strong physical reason for it. A better choice in this case (and perhaps also in the case of  $t'_1$ ) may be to take  $t'_2$  (and  $t'_1$ ) as the times at which  $\varepsilon$ , from (3.16), takes the value 0.5, since for smaller values of  $\varepsilon$ , (3.34) is expected to be very accurate (see p. 142). This would also be the only possible choice for a free stream that did not reverse its direction at  $t = T_1$ , but merely came close to zero, so that the quasi-steady expansion broke down. The results to be quoted were based on the choices (3.36a, b), but it was verified by Pedley (1976a) that  $\varepsilon$  lay between 0.4 and 0.6 for all take-overs, so the two methods of evaluating  $t'_1$  and  $t'_2$  are almost equivalent. This result follows from the fact that for a uniformly accelerating (or decelerating) flow, when  $U \equiv \pm t$ , then  $t'_1$  (or  $t'_2$ )  $\equiv (2x)^{1/2}$ , and  $\varepsilon$  is exactly equal to 0.5 at these times. The equivalence of the two methods would break down only for flows whose acceleration varied rapidly as the velocity passed through zero.

Somewhat different approximate methods have been used in the past to analyse unsteady boundary layers. Atabek & Chang (1961), in a discussion of unsteady entry flow in a tube, used the Oseen approximation, replacing the convective inertia terms in (3.32) by  $U(t)u_x$ . This makes the equation linear and therefore relatively easy to solve. However, while this might be expected to give an accurate description of the flow at the outer edge of the boundary layer, there are no grounds for supposing it to be a good approximation near the wall, where  $u \ll U$  and where the shear stress is calculated. The present method is certainly much more accurate in the approximately quasi-steady regime; it is unlikely to be significantly more inaccurate during the diffusive periods when  $U$  is small, and it is just as easy to use. A modified Oseen approximation was proposed by Lewis & Carrier (1949), who replaced the convective inertia terms by  $cUu_x$  for some constant  $c$  such that  $0 < c < 1$ . The quantity  $cU$

was to represent an average across the boundary layer of the convection velocity. These authors found that if  $c$  is taken equal to about 0.35, the Blasius value of wall shear was obtained for steady flow over a flat plate (although the predicted displacement thickness is in error by 11%). Carrier & Di Prima (1956) subsequently applied the method to small-amplitude oscillatory flow over a semi-infinite flat plate; it has the merit of giving the correct answer in steady flow, and of predicting a continuous velocity field. However, the method has not been used for large-amplitude oscillations, and there is no *a priori* way of knowing whether a constant value of  $c$  is appropriate throughout a flow reversal, or for different geometries (e.g. with an  $x$ -dependent outer flow).

Under the modified Oseen approximation, a change of variables to

$$w(\xi, y, t) = u(x, y, t) - U(t), \quad \xi = x - \int_0^t cU(t') dt'$$

reduces the problem of an unsteady flow starting from rest at  $t = 0$  to the solution of the one-dimensional diffusion equation for  $t > 0$ :

$$w_t = w_{yy}$$

with

$$w(\xi, \infty, t) = 0, \quad w_y(\xi, 0, t) = 0, \quad w(\xi, y, 0) = 0,$$

$$w(\xi, 0, t) = -U(t)H\left[\xi + \int_0^t cU(t') dt'\right],$$

where  $H$  is the Heaviside step function. This has the solution (in terms of  $u$  and  $x$  again)

$$\begin{aligned} u = U(t) - \frac{2}{\sqrt{\pi}} \int_{\eta_0}^{\infty} U\left[t\left(1 - \frac{\eta_0^2}{\mu^2}\right)\right] \\ \times H\left[x - \int_{t(1-\eta_0^2/\mu^2)}^t cU(t') dt'\right] e^{-\mu^2} d\mu, \end{aligned} \quad (3.37)$$

where

$$\eta_0 = y/2\sqrt{t}.$$

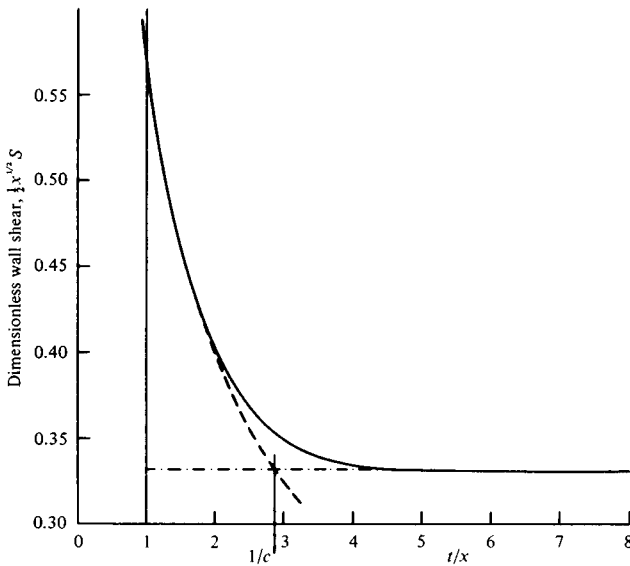


Fig. 3.5. Graph of dimensionless wall shear,  $\frac{1}{2}x^{1/2}S$ , against  $t/x$ , for the impulsively started flat plate ( $U=1$ ): continuous curve, exact numerical solution, calculated by Hall (1969); dashed curve, Rayleigh solution; dot-dash curve, Blasius solution. The method of Pedley (1976a) is equivalent to jumping from the Rayleigh to the Blasius solution at  $t/x = 1$ ; the modified Oseen solution makes the jump at  $t/x = 1/c$ .

In the case of the impulsively started flat plate, for which  $U \equiv H(t)$ , this reduces to

$$\begin{aligned} u &= \operatorname{erf} \left[ \frac{1}{2}y(1/t)^{1/2} \right] \quad \text{for } 0 < t < x/c \\ &= \operatorname{erf} \left[ \frac{1}{2}y(c/x)^{1/2} \right] \quad \text{for } t > x/c. \end{aligned}$$

This solution consists of the pure Rayleigh layer formed initially, but taken to extend until  $t = x/c$  not  $t = x$  as in the method proposed here; at  $t = x/c$ , the Rayleigh layer is taken over by an approximation to the Blasius layer. The values of wall shear predicted in this case are

$$\begin{aligned} S &= (\pi t)^{-1/2} \quad \text{for } 0 < t < x/c \\ &= (\pi x/c)^{-1/2} \quad \text{for } t > x/c, \end{aligned}$$

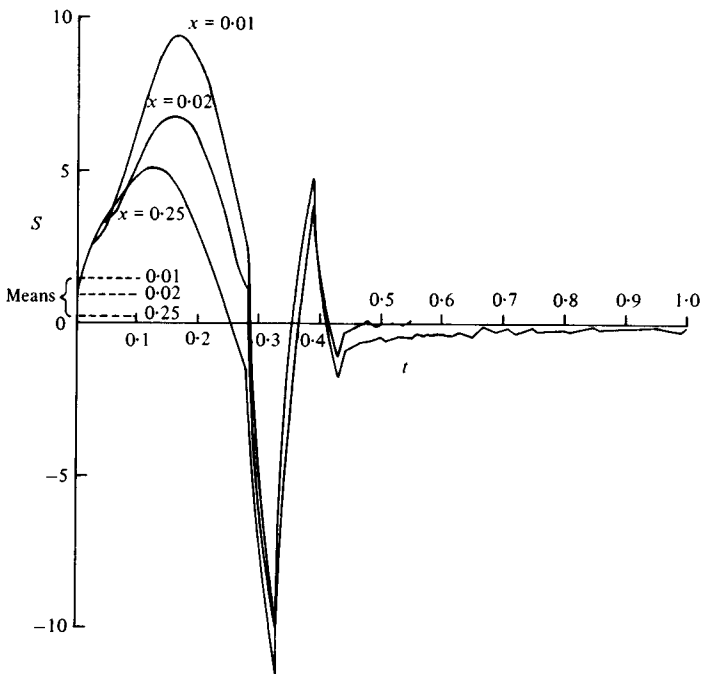


Fig. 3.6. Dimensionless shear-rate on the wall of the aorta, plotted against time, at three distances from the inlet. Motion in the boundary layer has almost completely died out by the end of the cycle. (After Pedley, 1976*a*.)

and agree more closely with the exact numerical values than the present method (fig. 3.5; I am grateful to Dr S. Farthing for pointing this out to me). The improvement essentially lies in choosing a more appropriate time for the take-over of the quasi-steady solution from the diffusive one, equivalent to multiplying the right-hand sides of equations (3.36) by  $c$ . The shear stress agrees with the exact solution in the quasi-steady region because  $c$  was chosen to make it do so. Whenever the modification to the quasi-steady shear (represented by the second term in (3.34)) is significant, the agreement will not be exact. On the other hand, in all cases, use of the modified Oseen solution means that the influence of convection will not be completely lost in the diffusive region, as in the present method. An improvement in the present method could therefore be made by keeping (3.34) in the quasi-steady regions, but using (3.37) instead

of (3.33) in the diffusive regions, the time origin of the diffusion still being determined by continuity of the displacement thickness. I would propose that the take-over times still be determined either by equations (3.36) or by the condition  $\varepsilon = 0.5$  (see (3.16)), except in cases of impulsively started steady motion when a different condition may lead to an improvement (cf. fig. 3.5).

According to the approximate theory of Pedley (1976*a*), the dimensionless wall shear is predicted to be

$$S = 2\pi^{-1/2} t^{1/2} \int_0^1 \dot{U}[t(1-\lambda^2)] d\lambda \quad \text{for } 0 < t < t'_1, \quad (3.38a)$$

$$S = [U^{3/2}(t)/(2x)^{1/2}][f''_0(0) + (x\dot{U}/U^2)f''_{11}(0)] \quad \text{for } t'_1 < t < t'_2, \quad (3.38b)$$

$$S = [\pi(t-t_0)]^{-1/2} \left\{ U(t'_0) + 2(t-t'_0) \times \int_0^1 \dot{U}[t-\lambda^2(t-t'_0)] d\lambda \right\} \quad \text{for } t'_2 < t < 1, \quad (3.38c)$$

where (3.38*b*) consists of the first two terms of (3.14). This quantity has been calculated for the case in which the free-stream velocity takes the form shown in fig. 3.3.  $S$  is plotted as a function of time for three different values of  $x$  in fig. 3.6. Very near the entrance ( $x = 0.01$ ) there is a large, quasi-steady peak in  $S$ , almost in phase with the peak velocity. This diminishes rapidly as  $x$  increases, and has an increasing phase lead, as one would expect from the theory of § 3.2.2. However, at all values of  $t$  or  $x$ , the shear-rates with the greatest magnitudes are negative. These high reversed shear-rates are a consequence of the large adverse pressure gradient associated with the rapid deceleration of the aortic core flow as the aortic valve closes. It can also be seen that in all cases the wall shear has almost completely died away at the end of the beat, confirming that the residual motions are very small and can be neglected in calculations of the oscillatory components of wall shear.

If  $x$  is too large, it is predicted that no quasi-steady regime exists, even at peak systole, because no fluid element that has passed the leading edge at any time during the cycle can arrive at  $x$  before the end of the cycle (i.e. (3.36*a*) has no solution). In the case considered



here, the critical value of  $x$  above which no quasi-steady solution exists is about 0.21 (corresponding to  $\hat{x} \approx 4.2$  cm). Thus the curve for  $x = 0.25$  in fig. 3.6 is calculated entirely from the first diffusive solution (3.38a), and the same curve would be predicted for all  $x$  greater than 0.21. This cannot be strictly true, because if the flow were independent of  $x$  the equations would be linear, and the mean flow (uncoupled from the oscillations) would be Poiseuille flow. But the steady entrance length for Poiseuille flow is approximately  $0.06 a Re$  (where  $a$  is the tube radius and  $Re$  is the Reynolds number), equal to about 33 cm in the present case. So the mean flow cannot be Poiseuille flow for all  $\hat{x}$  greater than 4.2 cm. The error in the present method lies in neglecting the residual motions at the end of each cycle; after many cycles these would build up (differently for each  $x$ ) and would lead to an  $x$ -dependent mean flow. The remedy consists simply in assuming that, for values of  $x$  greater than 0.21, the oscillatory and mean flows do not interact, as predicted by the theory of § 3.2.2. The oscillatory flow would be independent of  $x$ , consisting of a number of superimposed Stokes layers, and the associated wall shear could be calculated using either (3.1d) or (3.38a) (the two are equivalent if the boundary layers are thin, i.e. if the Womersley parameter,  $\alpha$ , is large). The mean flow would be steady entry flow, as described in § 3.2.1. Thus the present method is expected to predict the oscillatory components of wall shear accurately for all  $x$ , while giving increasingly inaccurate predictions of the mean shear as  $x$  increases up to the value 0.21; for  $x$  greater than 0.21, steady entry flow should predict the mean shear accurately.

We can see from fig. 3.6, as we saw in the case of fully developed flow in coronary arteries, that the amplitude of wall shear stress oscillations is predicted to be much larger than the mean shear. At  $x = 0.01$ , the mean shear is about 15% of the (negative) peak, compared with a mean velocity that is 17% of the (positive) peak velocity. However, this is predicted to fall rapidly, being 9% at  $x = 0.02$ , and reaching as little as 2% in fully developed flow. The r.m.s. value of  $S$ , on the other hand, falls from about 40% of the peak to about 30%, and remains considerably larger than the mean. In view of the large amplitudes of the oscillations in  $S$ , it seems much more likely *a priori* that the permeability of the artery wall, and thus

the generation of atherosclerosis, is correlated with some measure of wall shear that is independent of direction, like the peak or r.m.s. value, rather than the arithmetic mean. Finally, we note that  $S$  is non-dimensionalised with respect to  $U_0(\nu T)^{-1/2}$ , so in this case the peak wall shear-rate is about  $4000 \text{ s}^{-1}$ . This corresponds to a wall shear *stress* of  $16 \text{ N m}^{-2}$ , which is below that which causes endothelial damage ( $40 \text{ N m}^{-2}$ ; see § 1.2) but not by a huge factor.